Degradation of phenols by heterogeneous electro-Fenton with a Fe_3O_4-chitosan composite and a boron-doped diamond anode

Alberto A. Pujol[a], Itzel León[a], Jesús Cárdenas[a], Selene Sepúlveda-Guzmán[b], Juan Manríquez[a,#], Ignasi Sirés[c,#], Erika Bustos[a,*,#]

[a] *Centro de Investigación y Desarrollo Tecnológico en Electroquímica, S. C., CIDETEQ, Parque Tecnológico Querétaro S/N, Sanfandila, Pedro Escobedo, 76703 Querétaro, Mexico*

[b] *Universidad Autónoma de Nuevo León, UANL, Facultad de Ingeniería Mecánica y Eléctrica, FIME, Ave. Pedro de Alba s/n, Ciudad Universitaria, 66455 San Nicolás de los Garza, Nuevo León, Mexico*

[c] *Laboratori d'Electroquímica dels Materials i del Medi Ambient, Departament de Química Física, Facultat de Química, Universitat de Barcelona, Martí i Franquès 1-11, 08028 Barcelona, Spain*

Paper submitted to be published in ***Electrochimica Acta***

* Corresponding author: Tel.: +52 442 2 11 60 59; fax: +52 442 2 11 60 01.

E-mail address: ebustos@cideteq.mx (E. Bustos)

[#] Active ISE member

Abstract

Four phenolic compounds, either as single molecules or in mixtures, were treated by heterogeneous electro-Fenton using an undivided cell with a Ti mesh cathode, put in contact with a composite made of Fe_3O_4 nanoparticles (NPs) on chitosan (CS) made by chemical reduction, and a boron-doped diamond (BDD) anode. The removals attained upon the application of 2.3 V for 4 h to model solutions with 0.5 mol dm^{-3} H_2SO_4 as electrolyte were: 93% for phenol, 30% for *m*-chlorophenol, 24% for *o*-chlorophenol and 22% for *p*-chlorophenol. COD removal efficiencies reached 95% for phenol and *m*-chlorophenol, 88% for *p*-chlorophenol and 57% for *o*-chlorophenol. The degradation was feasible thanks to the production of hydroxyl radicals, both on the BDD surface (i.e., BDD($^{\bullet}$OH)) from water oxidation and in the bulk from Fenton's reaction. The composite cathode allowed the continuous H_2O_2 electrogeneration and Fe(III) reduction to Fe(II). The reaction between H_2O_2 and Fe(II) in solid or liquid phase yielded $^{\bullet}$OH. The disappearance of phenols was much slower in the absence of the composite catalyst.

Keywords: BDD anode; Chitosan; Electro-Fenton process; Magnetite; Phenol; Water treatment.

1. Introduction

Phenols are aromatic compounds containing one or more hydroxyl groups attached to the aromatic ring and contained in the wastewater of a variety of industries including oil refining, dye, and plastic manufacture, pulp and paper, and the pharmaceutical sector, among others [1-3], by this reason the Environmental Protection Agency (EPA) of the United States has also classified phenol and some phenolic compounds as priority pollutants [1-2].

Biological techniques have been commonly used to remove phenols from water. However, at a concentration higher than 200 mg dm^{-3} [4] these methods become ineffective and the microorganisms are completely deactivated at a concentration greater than 3 g dm^{-3} [1]. So, highly effective methods to treat bio-refractory pollutants, such as the so-called electrochemical advanced oxidation processes (EAOPs) [5-6] using boron-doped diamond (BDD) to its wide potential window, low background current and adsorption ability, and high corrosion resistance and efficiency in the electro-oxidation process compared with other electrodes [7-13], even though they are known to be expensive.

Among the EAOPs, electro-Fenton process (EF) is highly effective when it operates at acidic pH in the presence of H_2O_2 and ferrous ions, yielding a great amount of $^{\bullet}OH$ in the bulk [14]. EF can also be applied to water treatment at near-neutral pH, since it can employ either chelated iron [15] or iron in the solid form [16]. The latter version gives rise to a heterogeneous EF process [17]. Due to widespread availability, low toxicity, non-volatility, high stability and low cost, inverse spinel magnetite (Fe_3O_4) is a suitable heterogeneous Fenton catalyst [18-20]. First, it contains $Fe(II)_{magnetite}$ as an electron donor to initiate the

Fenton's reaction according to the classical Haber–Weiss mechanism. Second, the octahedral arrangement in the magnetite structure can easily accommodate both, Fe(II) and Fe(III), being Fe(II) reversibly oxidized and reduced within the same structure. Third, the isostructural substitution of iron by different transition metals can tune the physical-chemical properties of magnetites to produce more active systems. As suggested in the literature [18], oxygen competes with phenolic compounds to get the electrons from Fe(II), thus producing reactive oxygen species like $O_2^{\bullet-}$, H_2O_2 and $^{\bullet}OH$. Despite these benefits, scarce work has been carried out with magnetite in heterogeneous EF, whose main reactions (1)-(6) are:

$$Fe(II)_{magnetite} + O_2 \rightarrow O_2^{\bullet-} + Fe(III)_{magnetite} \quad (1)$$

$$Fe(II)_{magnetite} + O_2^{\bullet-} + 2H^+ \rightarrow Fe(III)_{magnetite} + H_2O_2 \quad (2)$$

$$O_2^{\bullet-} + H^+ \leftrightarrow HO_2^{\bullet} \quad (3)$$

$$2O_2^{\bullet-} + 2H^+ \rightarrow H_2O_2 + O_2 \quad (4)$$

$$Fe(II)_{magnetite} + H_2O_2 \rightarrow Fe(III)_{magnetite} + {}^{\bullet}OH + OH^- \quad (5)$$

$$O_2^{\bullet-} + H_2O_2 + H^+ \rightarrow O_2 + {}^{\bullet}OH + H_2O \quad (6)$$

In addition, $Fe(II)_{magnetite}$ may yield Fe^{2+}, promoting the classical Fenton's reaction with electrogenerated H_2O_2 as follows:

$$Fe(II)_{magnetite} \rightarrow Fe^{2+} \quad (7)$$

$$Fe^{2+} + H_2O_2 \rightarrow Fe^{3+} + {}^{\bullet}OH + {}^{-}OH \quad (8)$$

Several synthesized polymers [21-24], including polyvinyl alcohol, polyethylene glycol, polyamides, polyglycidyl methacrylate, polyacrylic acid and chitosan (CS) were employed as coating agents to modify the surface of the Fe_3O_4 nanoparticles (NPs). Although the polymeric coatings can minimize the

aggregation of the NPs, they may also increase the overall size of the particles and limit the expression of magnetic property [21]. In particular, CS is a polysaccharide produced by the deacetylation of chitin. Chitosan is a non-toxic, biodegradable and biocompatible material, and the second most abundant natural polymer in the world [25-26], by its physicochemical characteristics [25-31] is used in many environmental applications [32-35].

Based on the previous technologies employed to remove phenols from water, the main objective of this work is to assess the performance of heterogeneous EF with Fe_3O_4 NPs + CS composite as catalyst and BDD as the anode to degrade phenol and several chlorophenols from model solutions. To our knowledge, one work has been reported on the use of Fe_3O_4 NPs + CS in EF, aimed at removing a pesticide [36]. However, in the present investigation the catalyst was put in contact only with the Ti mesh cathode, in order to promote the generation of $Fe(II)_{magnetite}$ from $Fe(III)_{magnetite}$ reduction. The EF results were compared with electro-oxidation ones (i.e., in the absence of Fe_3O_4 NPs).

2. Experimental

2.1. Pre-activation and characterization of BDD anode

In this study, a 3-μm thick polycrystalline BDD ([B] = 1300 ppm) film was deposited on a titanium substrate by hot filament chemical vapor deposition (HF-CVD) [7]. These electrodes were purchased from Adamant Technologies. Activation of C-sp^3 sites on the surface through the elimination of C-sp^2 sites was achieved via anodic polarization at 1.83 mA cm^{-2} for 15 min in 0.5 mol dm^{-3}

H_2SO_4 (J.T. Baker, 95.4%) [8]. An undivided electrochemical cell with a BDD anode (geometric area of 21 cm^2) and a Ti mesh cathode (3.0 × 4.5 cm) was employed.

To characterize the ability of the BDD anode to produce $^{\bullet}OH$, coumarin degradation was monitored by UV/Vis spectrophotometry at a wavelength of 277 nm. The well-known equimolar reaction between coumarin and $^{\bullet}OH$ produces 7-hydroxycoumarin [37-38].

A calibration curve, at various concentrations of coumarin in 0.5 M H_2SO_4 (0.05-0.30 mM), was generated. The species changes during the electrolytic trials were monitored using a PerkinElmer Lambda XLS UV/Vis spectrophotometer within the range from 190 to 1100 nm. Solutions of 10 cm^3 of 0.12 mol dm^{-3} coumarin in 0.5 mol dm^{-3} H_2SO_4 were electrolyzed at 30 mA, supplied by a BASi Epsilon potentiostat, for 15 min under a constant stirring of 300 rpm, using a Pt wire as the auxiliary electrode [37-38].

2.2. Synthesis and characterization of Fe_3O_4 NPs

The synthesis of Fe_3O_4 NPs was performed by chemical reduction using water as the solvent [39]. Initially, a solution of 0.02 mol dm^{-3} $FeCl_3$ (J.T. Baker, 97%) was prepared and then 0.16 g of polyvinylpyrrolidone (PVP, Sigma-Aldrich, 98%) was added. The mixture was constantly stirred until a homogeneous solution was obtained. Finally, 0.059 g of $NaBH_4$ (J.T. Baker, 98%), as a reducing agent, was added. The synthesis was conducted at 80 °C to optimize the size of monodispersed Fe_3O_4 NPs (ϕ < 20 nm), as reported in the literature [23]. The resulting NPs were washed with 5 cm^3 H_2O, 5 cm^3 ethanol and 5 cm^3 acetone (J.T. Baker, 99.8%). A 5 min constantly stirred

magnetic separation was performed between each wash with a field strength of 11000 G. Finally, the Fe_3O_4 NPs were dried at room temperature for about 4 h.

The dispersion and size of Fe_3O_4 NPs were characterized using transmission electron microscopy (TEM) and selected area electron diffraction (SAED) by placing about 10 μL of the composite sample (a droplet) on a carbon-coated copper grid previously dried at room temperature. TEM and SAED measurements were made using a TITAN 80–300 transmission electron microscope operated at an accelerating voltage of 300 kV. The sizes of the nanoparticles, zeta potential, and electrical conductivity were measured using a Zetasizer Nano ZS90 instrument. The crystallographic features of the Fe_3O_4 NPs were assessed by X-ray diffraction (XRD) using a Thermo Scientific instrument.

2.3. Synthesis and characterization of the Fe_3O_4 NPs + CS composite

A small amount (1 g) of chitosan (CS, Aldrich, 99%) was dissolved in 100 cm^3 of 1% glacial acetic acid (J.T. Baker, 99.7%), then further stirred at 1000 rpm in an aqueous solution at pH 4.0. This reaction promoted the formation of a colloidal system with interstitial spaces filled by water molecules, as reported elsewhere [29,40] and following reaction (9).

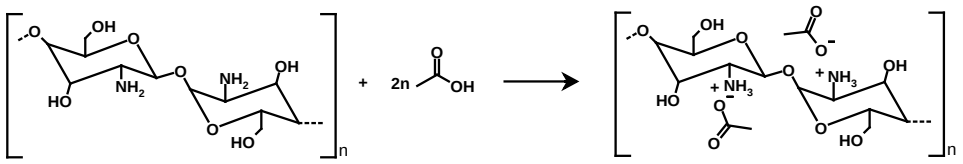

(9)

After the polymerization step, 333 mg of Fe_3O_4 NPs were added under mechanical mixing to uniformly disperse the NPs and the CS. Finally, 10 cm^3 of a 1 mol dm^{-3} NaOH (J.T. Baker, 98.3%) aqueous solution was added to form

the Fe_3O_4 NPs + CS gel microcomposite [27]. This prepared solution was injected drop by drop, using a syringe, into a 3 mol dm^{-3} NaOH gelling solution. The resulting hydrogel was filtered and conformed to obtain “balls” that were immersed into a bath containing 100 cm^3 of absolute ethylic alcohol (J.T. Baker, 99.5%) to produce Fe_3O_4 NPs + CS pellets with an average diameter of 1.5 cm (Figure 1).

To characterize the Fe_3O_4 NPs + CS composite, thin films, mixed with ethanol, were deposited on 304 stainless steel sheets, which were then dried at room temperature for 8 h. The films were characterized by UV/Vis spectrophotometry as well as FTIR spectroscopy taking as reference the CS alone. These results were compared with control samples prepared with CS hydrogel thin films without Fe_3O_4 NPs. The samples were analyzed using a Lambda XLS 057 instrument to record the UV/Vis spectra. Five single measurements were made and results were averaged. The characterization by FTIR was carried out with a Thermo Scientific Nicolet 6700 spectrometer. Equation (10) was used to compute the UV/Vis outset bandgap (ε_g), which is characteristic of the Fe_3O_4 NPs + CS composite because the Fe_3O_4 is considered as a semiconductor.

$$\varepsilon_g = (1240 \text{ eV nm}) / \lambda \qquad (10)$$

The production of H_2O_2 by the Fe_3O_4 NPs + CS composite or the CS or Ti was evaluated using semi-quantitative test strips from 1 to 100 mg dm^{-3} H_2O_2 using a Quantofix® Peroxide 100 by Macherey-Nagel GmbH & Co. KG., with reference 913 12.

2.4. Electrochemical degradation of phenols

The electrochemical degradation of dissolved samples of commercial TCI Merck (99%) phenol, *o*-, *m*- and *p*-chlorophenol was performed in an 80 cm^3 electrochemical cell, with a BDD anode and Ti mesh cathode (with the same dimensions mentioned above) put in electrical contact with the Fe_3O_4 NPs + CS composite (system denoted as BDD / (Fe_3O_4 NPs + CS)|Ti). Figure 1 shows the experimental setup, using approximately 35 g of composite in each experiment by the disponibility of space in the electrochemical cell. All the experiments were made by triplicate with good reproducibility of the results reusing the BDD / (Fe_3O_4 NPs + CS)|Ti system.

Samples containing each phenolic compound (10 mmol dm^{-3}) were electrolyzed in a 0.5 mol dm^{-3} H_2SO_4 medium. Polarization curves were obtained by chronopotentiometry for 15 min, at various DC cell potentials from equilibrium potential. The electrochemical degradation of the phenolic compounds was assessed by UV/Vis spectrophotometry, using the corresponding calibration curves. The removal percentages (% η) were calculated as reported in the literature [33-38].

The samples were characterized according to their pH, electrical conductivity (EC) and chemical oxygen demand (COD). The sample pH was measured with a Thermo Scientific Orion Star A215 potentiometer using a glass electrode. The EC was measured using a YSI 3200 conductometer, which was equipped with a YSI 3252 sensor (K_{cell} = 1 cm^{-1}). COD was evaluated, upon neutralization, in a Hach DRB200 digital reactor and Hach DR6000

spectrophotometer. The % η_{COD}, % $\eta_{\bullet OH}$ and % η_{H2O2} were calculated as reported in the literature [33-38].

3. Results and discussion

3.1. Characterization of the Fe_3O_4 NPs + CS composite

The average value of the outset bandgap (ε_g) of the Fe_3O_4 NPs + CS was 2.94 eV. This agrees with the results found in the literature (between 2.84 and 3.00 eV) [39-40], which allows distinguishing it from Fe_2O_3 since its bandgap should be between 1.6 and 2.2 eV [41]. This result confirms that the nanoparticles are composed of magnetite. They also showed a plasmon peak at 310 nm (Supplementary information, Figure 1A). Nanoparticle average diameters ranged as follows: 45% were smaller than 20 nm, 32% were between 20 and 50 nm, and 13% were greater than 50 nm, as can be seen in Figure 1B from supplementary information. In addition, they had an apparent zeta potential of -19.00 $\pm$ 8.26 mV (Supplementary information, Figure 1C) and electrical conductivity of 3.76 mS cm^{-1}.

Fe_3O_4 NPs ($\leq$ 20 nm) was confirmed by TEM analysis (Supplementary information, Figure 2A). Some agglomeration can be observed. The corresponding SAED analysis yielded several diffraction spots related to the magnetite crystalline structure including the (220), (311), (400), (440) and (511) planes (Supplementary information, Figure 2B). The crystalline structure was further corroborated by the XRD analysis (Supplementary information, Figure 2C), showing the characteristic diffraction peaks of magnetite at 2θ values of 30º, 35º, 43º, 57º and 63º (inset), as expected [42].

Results of FTIR spectrometry for the composite (Supplementary information, Figure 3) offer evidence of the presence of magnetite, as deduced from the appearance of the characteristic signals at 3616 cm^{-1}, which is related to the O-H stretching at CS adsorbed on the surface of the Fe_3O_4 NPs (Supplementary information, Table 1). Additionally, one can observe different stretching signals of CS derived from different functional groups: C-H (2988 cm^{-1}), N-H (1682 cm^{-1}), C-N by the amine group (1497 cm^{-1}) and C-O by the ether group (1182 cm^{-1}). For the Fe_3O_4 NPs, Fig. 4 shows their characteristic molecular vibrations at 794 and 677 cm^{-1} [43]. A proposal for the cation-pi interaction between the Fe_3O_4 NPs and CS is shown in Fig. 5. The CS has a partially negatively charged oxygen atom able to interact with the Fe_3O_4 NPs, which presented the apparent zeta potential of -19.00 $\pm$ 8.26 mV and electrical conductivity of 3.76 mS cm^{-1}, as mentioned above.

3.2. Electrochemical treatment of phenolic solutions

The spectra of the four phenolic compounds were obtained to verify their activity in the UV range. A $\pi \rightarrow \pi^*$ electronic transition can be observed between 270 and 280 nm (Supplementary information, Figure 4). By monitoring the signal around 270 nm, the calibration curves were obtained (Supplementary information, Figure 4E), reaching a good sensitivity and $R^2 > 0.94$ (Table 2 from supplementary information). The characteristic absorption of olefins and aromatic compounds, with signals between 200 and 300 nm and molar absorptivity from 1000 to 13000 cm^{-1} mol^{-1} dm^3 [44], is also evidenced in Table 2 from supplementary information. These results were used to monitor the efficiency of the removal of phenolic compounds upon electrochemical

generation of different kinds of hydroxyl radicals. Aiming to assess the water oxidation at BDD when very positive potentials are applied, the observed current has been suggested as an important parameter. During the electrolysis of phenolic compounds, the main expected pathway is the generation of adsorbed BDD($^{\bullet}$OH) and its further attack over the organic molecule. A current related to the oxidation process can be measured using chronoamperometry, where the current is recorded as a function of time during the application of a potential pulse [45].

To perform this study, the current at a fixed time τ (sampled current) was plotted as a function of the applied potential. The current-potential (*I* vs. *E*) curves obtained are presented in Figure 3. These results show the presence of each phenolic compound in the study [45]. Two systems were employed for comparison: in Figure 3A, BDD / (Fe_3O_4 NPs + CS)|Ti, and in Figure 3B, the same but without Fe_3O_4 NPs. In these figures, three zones can be distinguished [45,46]:

- *Zone I*: the oxidation is controlled by charge transfer (kinetic control); in this zone (0.2 to 1.0 V) the phenolic compounds do not show electroactivity yet, inducing any faradaic current;
- *Zone II*: mixed control (electron transfer and mass transport) predominates, involving potentials at which phenolic compounds are oxidized (1.2 to 2.0 V) but not so effectively that their surface concentration is zero;
- *Zone III:* the oxidation process is controlled by the rate at which the species reach the anode (mass transport control); the occurrence of water electrolysis (2.2 to 3.0 V) with the corresponding generation of

adsorbed hydroxyl radicals. The oxidation occurs at the highest speed for mass transport conditions at 2.3 V [45] by the evolution of O_2.

The current generated in the electrochemical cell in the presence of the Fe_3O_4 NPs composite (i.e., BDD / phenolic compounds / (Fe_3O_4 NPs + CS)|Ti) was higher than 0.06 mA, as shown in Figure 3A. In contrast, without the Fe_3O_4 NPs + CS composite (i.e., BDD / phenolic compounds / Ti) a lower current was obtained; lower than 0.22 mA (Figure 3B). These results demonstrate the conductivity of the magnetite nanoparticles, in contact with the Ti mesh, and their ability to enable significant oxidation of phenolic compounds. Here maximum hydroxyl radical production was observed at 2.3 V, by the evolution of O_2, as suggested by the presence of important phenolic degradation compound species in aqueous solution. Their generation, at high potential, is in accordance with the results reported in the literature [12, 46-47]. For this reason, the removals of aromatic compounds in this study were attained upon the application of 2.3 V for 4 h to model solutions with 0.5 mol dm^{-3} H_2SO_4.

The $^{\bullet}OH$ radical production in the H_2SO_4 supporting electrolyte increased with time just to 10 min. Samples at 5, 10 and 15 min were analyzed, as shown in Figure 4A, and the corresponding absorption spectra are depicted (Supplementary information, Figure 5A, and 5B). As can be seen, at 10 min, the % $\eta_{^{\bullet}OH}$ was higher using the BDD / (Fe_3O_4 NPs + CS)|Ti system (55%). With the BDD / (CS)|Ti system, the value was 37%. In both cases, the electrolyzes were carried out at a potential difference of 2.3 V between the anode and cathode.

On the other hand, Figure 4B shows the accumulation of H_2O_2 in both systems, whereas Figures 6A and 6B from the supplementary information

present the appearance of the strips employed to detect the chemical in each case at different times. It is important to consider that what was determined in these tests was the accumulated H_2O_2 since it partly reacts with Fe (II)$_{magnetite}$ in the solid phase (reaction (5)) and Fe^{2+} in a liquid phase (reaction (8)). It is clear that the presence of H_2O_2 can be disregarded in the absence of Fe_3O_4 NPs, whereas it was clearly formed in the BDD / (Fe_3O_4 NPs + CS)|Ti system. Using the semi-quantitative test strips Quantofix® Peroxide 100, a % η_{H2O2} of 33% was obtained after 5 min at 2.3 V, increasing up to 100% at 10 and 15 min with the latter system. Thus, the absence of H_2O_2 without using Fe_3O_4 indicates that there is no significant reduction of O_2 in the cathode and hence, the O_2 reduction on Ti is excluded.

The increase in the removal efficiency of phenolic compounds in synthetic samples during an extended 240 min test interval is shown in Figure 5. At 30 min, the BDD / (CS)|Ti system yielded removals of 37% and 5% for phenol and *p*-chlorophenol (Figure 5A). A faster disappearance was achieved by heterogeneous EF with the BDD / (Fe_3O_4 NPs + CS)|Ti system (Figure 5B), reaching 60% and 12% for the same pollutants at the same time. Additionally, for *m*-chlorophenol, after 180 min, close to double removal efficiency was observed in the arrangement with Fe_3O_4 NPs (30%, Figure 5B), since only 13% was observed in the uncatalyzed treatment. In the case of the *o*-chlorophenol, conversely, the removal efficiency at 240 min was higher in the arrangement without Fe_3O_4 NPs (Figure 5A) than with Fe_3O_4 NPs (Figure 5B) by the possible more easy absorption of this aromatic compound in the ortho position of chloro atom than, metha and para position of this functional group, at it has been reported before [48].

The removal efficiency of the phenolic compounds in this research was also evaluated in terms of COD (Table 1). The observed COD abatements using the heterogeneous EF process at 2.3 V for 240 min were: 95% for phenol and *m*-chlorophenol solutions > 88% for *p*-chlorophenol > 57% *o*-chlorophenol, accompanied by a decrease of electrical conductivity close to 350 mS cm^{-1} for the different solutions under, which is possible by the presence of CS. The role of phenolic compounds adsorption on either the CS or the composite was also assessed. Only 4% adsorption was found as maximum and hence, the disappearance of the pollutants and their degradation intermediates was due to the action of hydroxyl radicals.

Based on these results, the proposed reaction mechanism for the heterogeneous EF treatment of phenols is depicted in Figure 6. The electrochemical degradation using a BDD anode proceeds through the generation of BDD(•OH) from water oxidation, combined with the continuous cathodic reduction of $[Fe^{III}(Fe^{III})_2O_4]^+$ to $[Fe^{II}(Fe^{III})_2O_4]$. In the presence of O_2, $[Fe^{II}(Fe^{III})_2O_4]$ is partly re-oxidized in concomitance with H_2O_2 generation. As a result, H_2O_2 can produce •OH via Fenton's reaction, reacting either with Fe(II) in solid form or dissolved Fe^{2+}. All these radicals caused the gradual destruction of phenols, whose pre-concentration at the composite surface allowed the minimization of the mass transport limitations that usually account for slow degradation kinetics.

4. Conclusions

Model solutions of phenol and *o*-, *m*- or *p*-chlorophenol were effectively decontaminated by heterogeneous EF with a Fe_3O_4 NPs + CS composite as

catalyst, thanks to the simultaneous production of BDD(•OH) from water electro-oxidation and •OH from Fenton's reaction. The removals attained upon the application of 2.3 V for 4 h to model solutions were: 93% for phenol > 30% for *m*-chlorophenol > 24% for *o*-chlorophenol > 22% for *p*-chlorophenol. It was possible to reach COD abatements increasing in the following order: *o*-chlorophenol (57 %) > *p*-chlorophenol (88 %) > phenol and *m*-chlorophenol (95 %). These results were obtaining by the electrocatalytic effect of the system BDD/(Fe_3O_4 NPs + CS)/Ti considering the average value of the outset bandgap (ε_g) of the Fe_3O_4 NPs + CS of 2.94 eV with a plasmon peak at 310 nm and a nanoparticle average diameters $\leq$ 20 nm and an apparent zeta potential of -19.00 $\pm$ 8.26 mV with an electrical conductivity of 3.76 mS cm^{-1}. Additionally, the magnetite crystalline structure was confirm by the (220), (311), (400), (440) and (511) planes showing the characteristic diffraction peaks of magnetite at 2θ values of 30º, 35º, 43º, 57º and 63º (inset).

Acknowledgments

The authors acknowledge financial support from the Consejo Nacional de Ciencia y Tecnología (CONACyT, Mexico). The English revision from Richard Lindeke, Ph. D., Profesor Emeritus, University of Minnesota Duluth, as well as help from S.V. Trinidad, M.C. Cortés, M. Quijano, F.A. Robles and J.A. García is also acknowledged. A.A. Pujol Pozo and I. León thank CONACyT for its support to carry out their Doctoral and Master studies, respectively.

References

[1] H. Jiang, Y. Fang, Y. Fu, Q. –X. Guo, Studies on the extraction of phenol in wastewater, J. Hazard. Mater. B101 (2003) 179.

[2] Y. Han, X. Quan, Sh. Chen, H. Zhao, Ch. Cui, Y. Zhao, Electrochemically enhanced adsorption of phenol on activated carbon fibers in basic aqueous solution, J. Colloid Inter. Sci. 299 (2006) 766.

[3] A. Nuhoglu, B. Yalcin, Modelling of phenol removal in a batch reactor, Proc. Biochem. 40 (2005) 1233.

[4] X. Hao, M. Pritzker, X. Feng, Use of pervaporation for the separation of phenol from dilute aqueous solutions, J. Memb. Sci. 335 (2009) 96.

[5] I. Sirés, E. Brillas, M. A. Oturan, M. A. Rodrigo, M. Panizza, Electrochemical advanced oxidation processes: today and tomorrow. A review, Environ. Sci. Pollut. Res. 21 (2014) 8336-8367.

[6] C. A. Martínez-Huitle, M. A. Rodrigo, I. Sirés, O. Scialdone, Single and coupled electrochemical processes and reactors for the abatement of organic water pollutants: A critical review, Chem. Rev. 115 (2015) 13362-13407.

[7] A. Fujishima, T. Narasinga, New directions in structuring and electrochemical applications of boron–doped diamond thin films, Diamond Relat. Mater. 10 (2001) 1799.

[8] A. Medel, E. Bustos, L. M. Apátiga, Y. Meas, Surface activation of C-sp^3 in boron-doped diamond electrode, Electrocatalysis 4 (2013) 189.

[9] A. Galia, S. Lanzalaco, M. A. Sabatino, C. Dispenza, O. Scialdone, I. Sirés, Crosslinking of poly(vinylpyrrolidone) activated by electrogenerated hydroxyl radicals: A first step towards a simple and

cheap synthetic route of nanogel vectors, Electrochem. Commun. 62 (2016) 64-68.

[10] P. –A. Michaud, M. Panizza, L. Ouattara, T. Diaco, G. Foti, Ch. Comninellis, Electrochemical oxidation of water on synthetic boron – doped diamond thin film anodes, J. Appl. Electrochem. 33 (2003) 151.

[11] A. Medel, E. Bustos, K. Esquivel, L. A. Godínez, Y. Meas, Electrochemical incineration of phenolic compounds from the hydrocarbon industry using boron-doped diamond electrodes, Int. J. Photoenergy 2012 (2012) 681875.

[12] A. Bedolla-Guzman, I. Sirés, A. Thiam, J. M. Peralta-Hernández, S. Gutiérrez-Granados, E. Brillas, Application of anodic oxidation, electro-Fenton and UVA photoelectro-Fenton to decolorize and mineralize acidic solutions of Reactive Yellow 160 azo dye. Electrochim. Acta 206 (2016) 307-316.

[13] R. Oriol, M. P. Bernícola, E. Brillas, P. L. Cabot, I. Sirés, Paired electro-oxidation of insecticide imidacloprid and electrodenitrification in simulated and real water matrices, Electrochim. Acta 317 (2019) 753-765.

[14] E. Brillas, I. Sirés, M. A. Oturan, Electro-Fenton process and related electrochemical technologies based on Fenton's reaction chemistry, Chem. Rev. 109 (2009) 6570-6631.

[15] Y. C. Li, L. G. Bachas, D. Bhattacharyva, Kinetics studies of trichlorophenol destruction by chelate-based Fenton reaction, Environ. Eng. Sci. 22 (2005) 756.

[16] I. S. X. Pinto, P. H. V. V. Pacheco, J. V. Coelho, E. Lorençon, J. Ardisson, J. D. Fabris, Nanostructured δ-FeOOH: An efficient Fenton-like

catalyst for the oxidation of organics in water, Appl. Catal. B: Environ. 119 (2012) 175.

[17] S. O. Ganiyu, M. Zhou, C. A. Martínez-Huitle, Heterogeneous electro-Fenton and photoelectro-Fenton processes: A critical review of fundamental principles and application for water/wastewater treatment, Appl. Catal. B: Environ. 235 (2018) 103-129.

[18] G. –D. Fang, D. –M. Zhou, D. D. Dionysiou, Superoxide mediated production of hydroxyl radicals by magnetite nanoparticles: demonstration in the degradation of 2-chlorobipheyl, J. Hazard. Mater. 250-251 (2013) 68.

[19] R. C. C. Costa, F. C. C. Moura, J. D. Ardisson, J. D. Fabris, R. M. Lago, Highly active heterogeneous Fenton-like systems based on Fe/Fe_3O_4 composites prepared by controlled reduction of iron oxides, Appl. Catal. B: Environ. 83 (2008) 131.

[20] L. Xu, J. Wang, Magnetic nanoscaled Fe_3O_4/CeO_2 composite as an efficient Fenton-like heterogeneous catalyst for degradation of 4-chlorophenol, Environ. Sci. Technol. 46 (2012) 10145.

[21] Y. Wei, B. Han, X. Hu, Y. Lin, X. Wang, X. Deng, Synthesis of Fe_3O_4 nanoparticles and their magnetic properties, Proc. Eng. 27 (2012) 632.

[22] K. Tao, H. J. Dou, K. Sun, Interfacial coprecipitation to prepare magnetite nanoparticles: Concentration and temperature dependence, Col. Surf. 320 (2008) 115.

[23] S. F. Si, C. H. Li, X. Wang, D. P. Yu, Q. Peng, Y. D. Li, Magnetic monodisperse Fe_3O_4 nanoparticles, Cryst. Growth Des. 5 (2005) 391.

[24] Y. Ding, Y. Hu, L. Y. Zhang, Y. Chen, X. Q. Jiang, Synthesis and magnetic properties of biocompatible hybrid hollow spheres, Biomacromol. 7 (2006) 1766.

[25] B. Krajewska, Application of chitin-and chitosan-based materials for enzyme immobilizations: A review, Enzym. Microbiol. Technol. 35 (2004) 126.

[26] C. K. S. Pillai, W. Paul, C. P. Sharma, Chitin and chitosan polymers: Chemistry, solubility and fiber formation, Progr. Polym. Sci. 34 (2009) 641.

[27] L. Zang, X. Qiao, L. Hu, Ch. Yang, Q. Liu, Ch. Wei, J. Qiu, H. Mo, G. Song, J. Yang, Ch. Liu, Preparation and evaluation of coal fly ash / chitosan composites as magnetic supports for highly efficient cellulose immobilization and cellulose bioconversion, Polymers 10 (2018) 2.

[28] A. Boujemaoui, S. Mongkhontreerat, E. Malmstr€om, A. Carlmark, Preparation and characterization of functionalized cellulose nanocrystals, Carbohydr. Polym. 115 (2015) 457.

[29] V. S. Yeul, S. S. Rayalu, Unprecedented chitin and chitosan: a chemical overview, J. Polym. Environ. 21 (2013) 606.

[30] R. K. Mishra, S. K. Ha, K. Verma, S. K. Tiwari, Recent progress in selected bio-nanomaterials and their engineering applications: an overview, J. Sci. Adv. Mater. Dev. (2018) 1.

[31] C. M. Futalan, C. C. Kan, M. L. Dalida, K. J. Hsien, C. Pascua, M. W. Wan, Comparative and competitive adsorption of copper, lead, and nickel using chitosan immobilized on bentonite, Carbohydr. Polym. 83 (2011) 528.

[32] M. N. Kumar, R. A. Muzzarelli, C. Muzzarelli, H. Sashiwa, A. J. Domb, Chitosan chemistry and pharmaceutical perspectives, Chem. Rev. 104 (2004) 6017.

[33] S. Hirano, Chitin biotechnology applications, Biotechnol. Ann. Rev. 2 (1996) 237.

[34] S. Demarger-Andre, A. Domard, New properties of chitosan in lipid dispersions, in: Z. S. Karnicki, A. Wojtaso Pajak, M. M. Breziski, P. J. Bylowski (Eds.), Chitin World, Bremerhauser, Germany, 1994, p. 153.

[35] R. W. Coughlin, M. R. Deshaies, E. M. Davis, Preparation of chitosan for heavy metal removal, Environ. Progress 9 (1990) 35.

[36] S. Rezgui, A. Amrane, F. Fourcade, A. Assadi, L. Monser, N. Adhoum, Electro-Fenton catalyzed with magnetic chitosan beads for the removal of Chlordimeform insecticide, Appl. Catal. B: Environ. 226 (2018)346-359.

[37] R. Herrada, A. Medel, F. Manríquez, I. Sirés, E. Bustos, Preparation of IrO_2-Ta_2O_5|Ti electrodes by immersion, painting and electrophoretic deposition for the electrochemical removal of hydrocarbons from water, J. Hazard. Mater. 319 (2016) 102.

[38] R. A. Herrada, G. Acosta-Santoyo, S. Sepúlveda-Guzmán, E. Brillas, I. Sirés, E. Bustos, IrO_2-Ta_2O_5 | Ti electrodes prepared by electrodeposition from different Ir:Ta ratios for the degradation of polycyclic aromatic hydrocarbons, Electrochim. Acta 263 (2018) 353.

[39] H. Gobara, I. Nassar, A. Naggar, G. Eshaq, Nanocrystalline spinel ferrite for an enriched production of hydrogen through a solar energy stimulated water splitting process, Energy 118 (2017) 1234.

[40] H. El Ghandoor, H. Zidan, M. Khalil, M. Ismail, Synthesis and some physical properties of magnetite (Fe_3O_4) nanoparticles, Intern. J. Electrochem. Sci. 7 (2012) 5734.

[41] W. Strehlow, E. Cook, Compilation of energy band gaps in elemental and binary compound semiconductors and insulators, J. Phys. Chem. Ref. Data 2 (1973) 163.

[42] 87-2334 JCPDS -International Centre for Diffraction Data (2000). PCPDFWIN v 2.1.

[43] X. N. Pham, T. P. Nguyen, T. N. Pham, T. T. N. Tran, T. V. T. Tran, Synthesis and characterization of chitosan-coated magnetite nanoparticles and their application in curcumin drug delivery, Adv. Nat. Sci. Nanosci. Nanotech. 7 (2016) 3.

[44] J. R. Dyer, Aplicaciones de Espectroscopía de Absorción en Compuestos Orgánicos. Editorial Prentice / Hall International, New Jersey, 1973.

[45] A. Bard, L. Faulker, Electrochemical methods fundamentals and applications, John Wiley and Sons, New York, 2000 (Second edition).

[46] B. Marselli, J. García, P. Michaud, M. Rodrigo, Ch. Comninellis, Electrogeneration of hydroxyl radicals on boron-doped diamond electrodes, J. Electrochem. Soc. 150 (2003) D79.

[47] P. Michaud, M. Panizza, L. Ouattara, T. Diaco, G. Foti, Ch. Comninellis, Electrochemical oxidation of water on synthetic boron-doped diamond thin film anodes, J. Appl. Electrochem. 33 (2003) 151.

[48] Z. N. Garba, W. Zhou, I. Lawan, W. Xiao, M. Zhang, L. Wang, L. Chen, Z. Yuan, An overview of chlorophenols as contaminants and their

removal from wastewater by adsorption: a review, J. Environ. Manag. 241 (2019) 59.

Figure and Table captions

Figure 1. Experimental setup for the electrochemical degradation of phenolic compounds in 0.5 mol dm^{-3} H_2SO_4, comprising: an undivided cell, with a central BDD plate as the anode and a Ti mesh in contact with the composite (Fe_3O_4 NPs + CS) as the cathode. Both electrodes are connected to a potentiostat for constant current supply.

Figure 2. Suggested chemical interaction between Fe_3O_4 NPs and CS.

Figure 3. Current-potential (*I* vs. *E*) curves in 10 mmol dm^{-3} of each phenolic compound in 0.5 mol dm^{-3} H_2SO_4 using two systems: (A) BDD (working electrode) and (Fe_3O_4 NPs + CS)|Ti (counter electrode); (B) same system, without the Fe_3O_4 NPs. The values were obtained by chronopotentiometry.

Figure 4. Time course of $\eta_{\bullet OH}$ (A) and η_{H2O2} (B) upon the application of 2.3 V between the anode and cathode, in a 0.5 mol dm^{-3} H_2SO_4 in the absence and presence of Fe_3O_4 NPs.

Figure 5. Relationship between η and *time* for the treatment of a mixture containing 10 mmol dm^{-3} of each phenol in 0.5 mol dm^{-3} H_2SO_4 using two systems: (A) BDD / (CS)|Ti and (B) BDD / (Fe_3O_4 NPs + CS)|Ti.

Figure 6. Schematic representation of the main steps involved in the electrochemical degradation of the mixture of phenols using the BDD / (Fe_3O_4 NPs + CS)|Ti cell.

Table 1. COD and Electrical Conductivity (EC) values before (COD_i, EC_i) and after (COD_f, EC_f) the electrolysis of phenolic pollutants in 0.5 mol dm^{-3} H_2SO_4

as supporting electrolyte using the BDD / (Fe_3O_4 NPs + CS)|Ti cell upon application of 2.3 V between the anode and cathode for 4 h. The corresponding removal efficiencies using the COD (% η_{COD}) values are also provided.

Figure 1

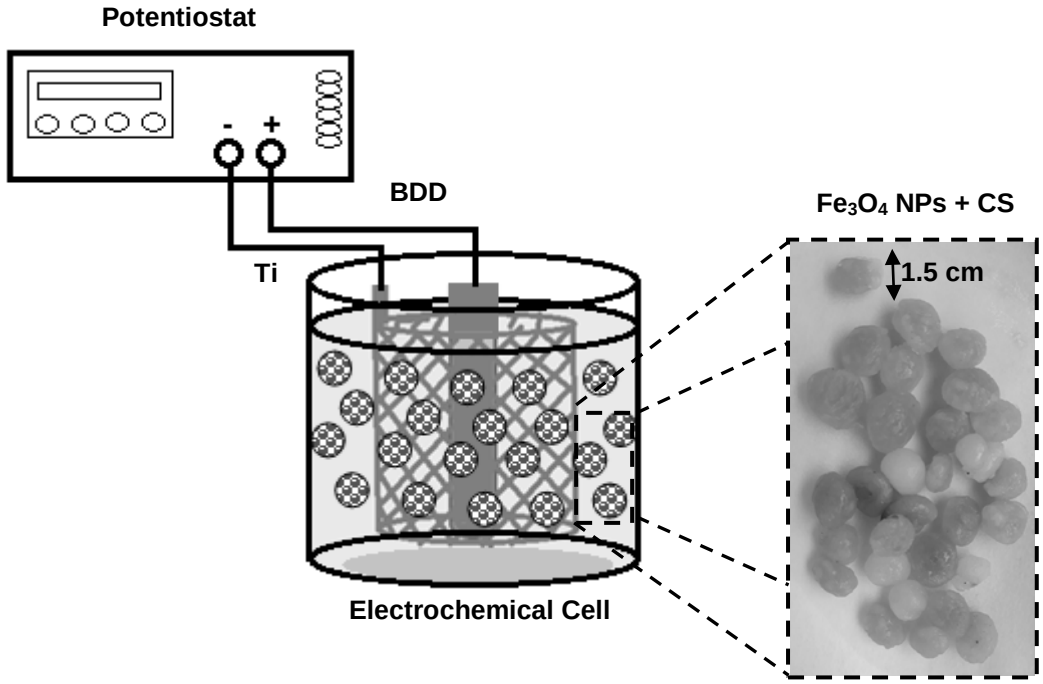
Potentiostat
-
+
BDD
Ti
Fe3O4 NPs + CS
1.5 cm
Electrochemical Cell

Figure 2

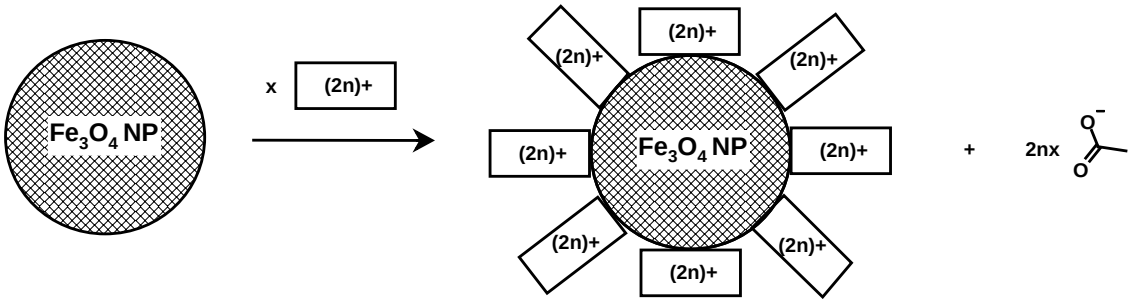

where :

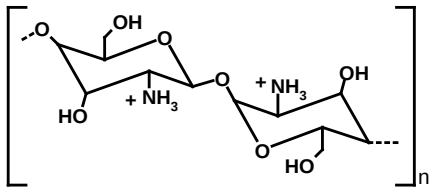

=

(2n)+

Figure 3

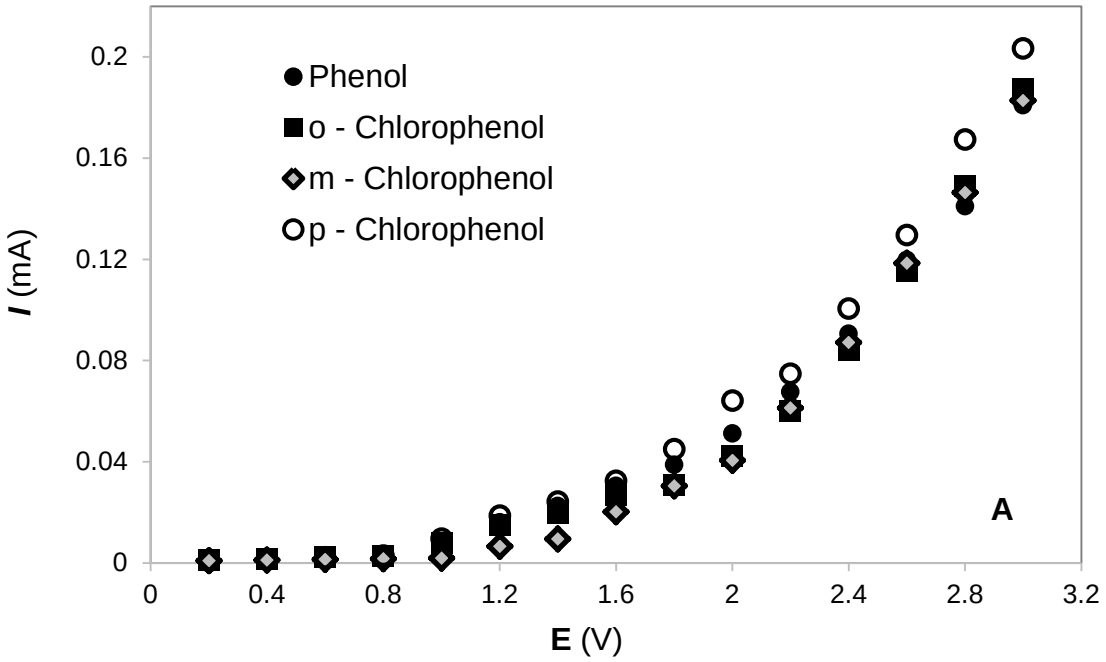
Phenol
o - Chlorophenol
m - Chlorophenol
p - Chlorophenol
I (mA)
E (V)
A
0
0.04
0.08
0.12
0.16
0.2
0.4
0.8
1.2
1.6
2
2.4
2.8
3.2

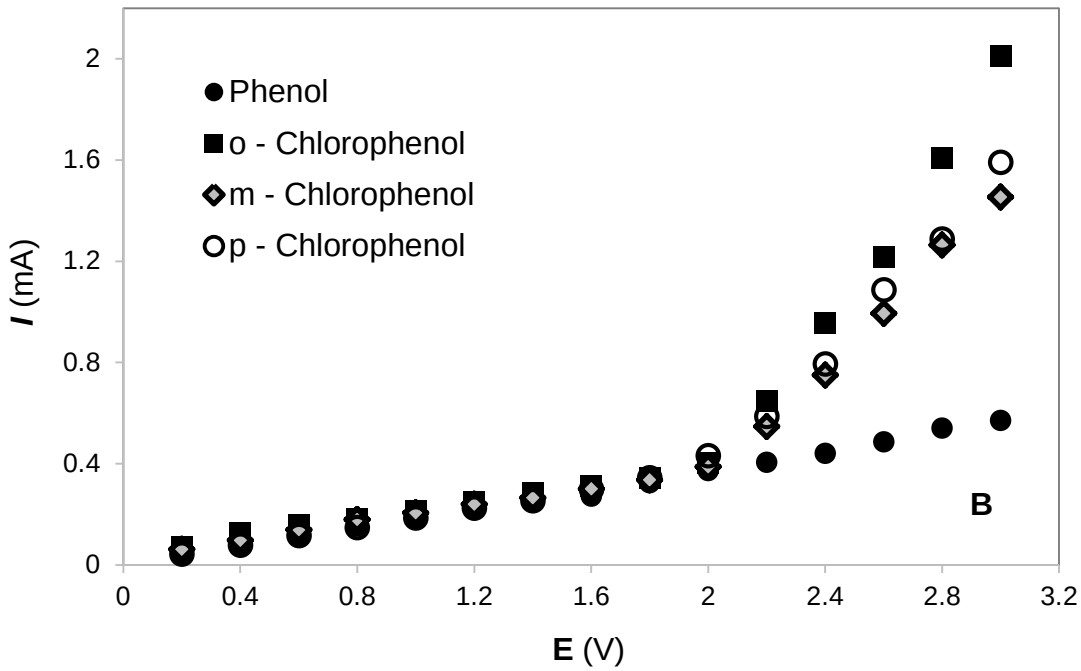
Phenol
o - Chlorophenol
m - Chlorophenol
p - Chlorophenol
I (mA)
E (V)
B
0
0.4
0.8
1.2
1.6
2
2.4
2.8
3.2

Figure 4

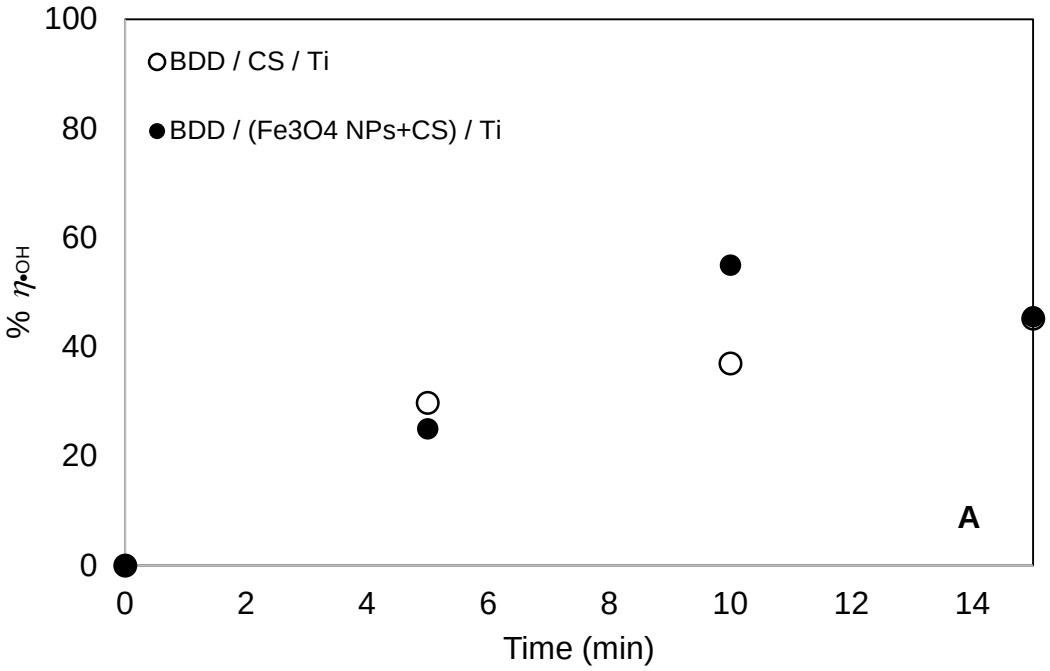
100
80
60
40
20
0
% $\eta_{\bullet OH}$
BDD / CS / Ti
BDD / (Fe3O4 NPs+CS) / Ti
A
0
2
4
6
8
10
12
14
Time (min)

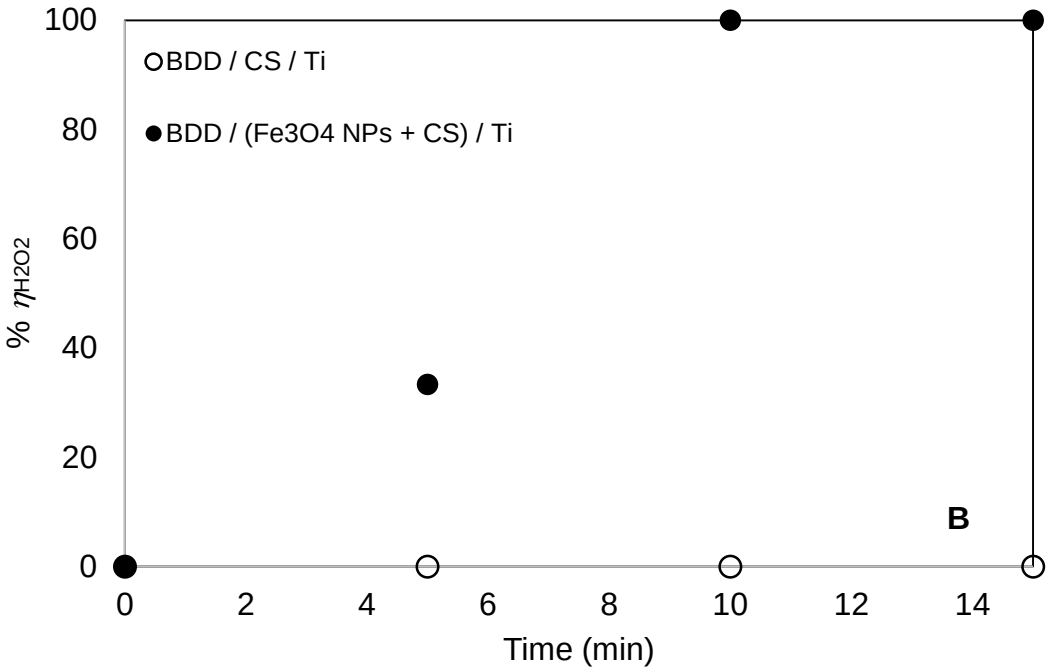
100
80
60
40
20
0
% η_{H2O2}
BDD / CS / Ti
BDD / (Fe3O4 NPs + CS) / Ti
B
0
2
4
6
8
10
12
14
Time (min)

Figure 5

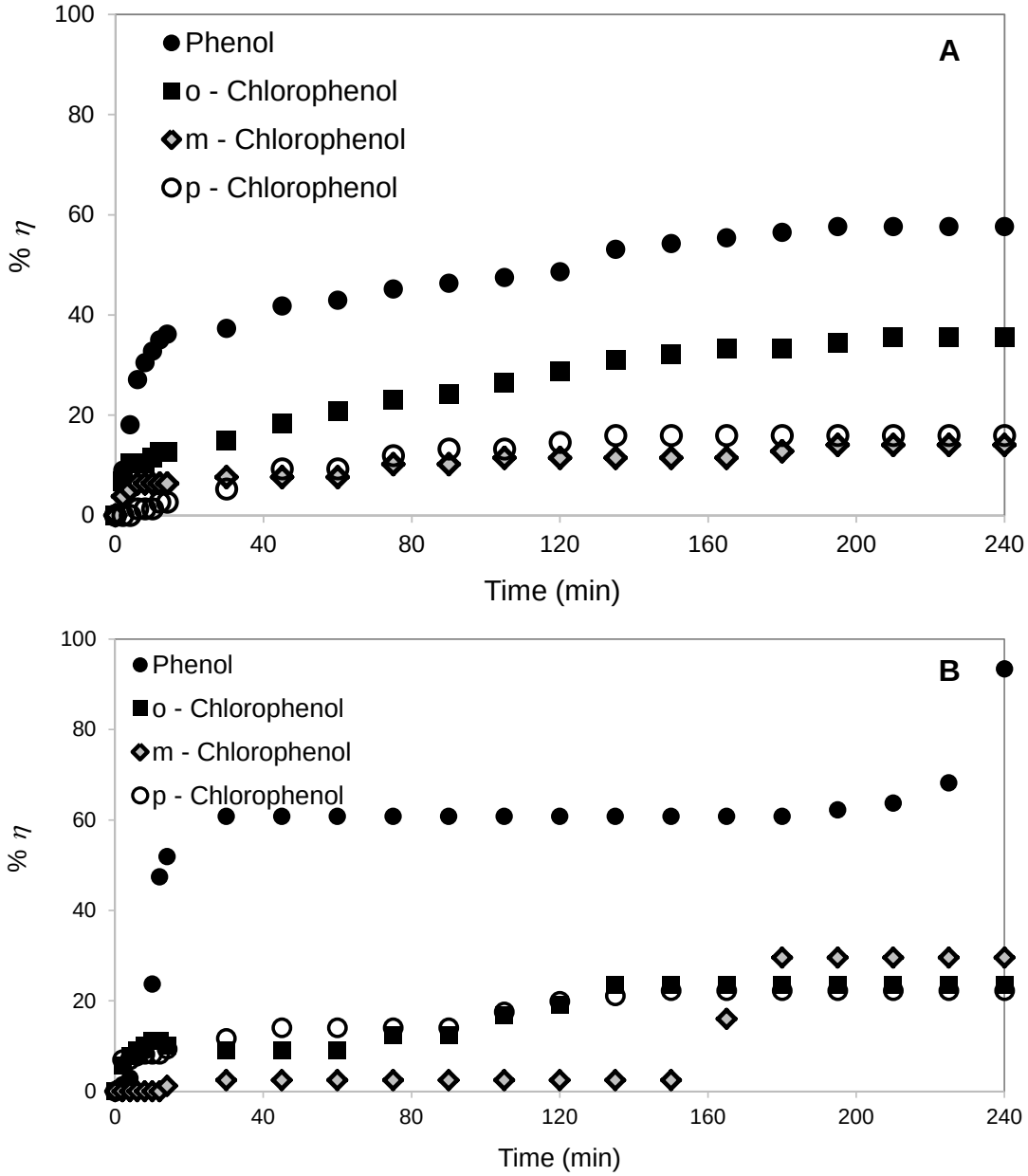
Phenol
o - Chlorophenol
m - Chlorophenol
p - Chlorophenol
A
% η
Time (min)
B
0
20
40
60
80
100
120
160
200
240

Figure 6

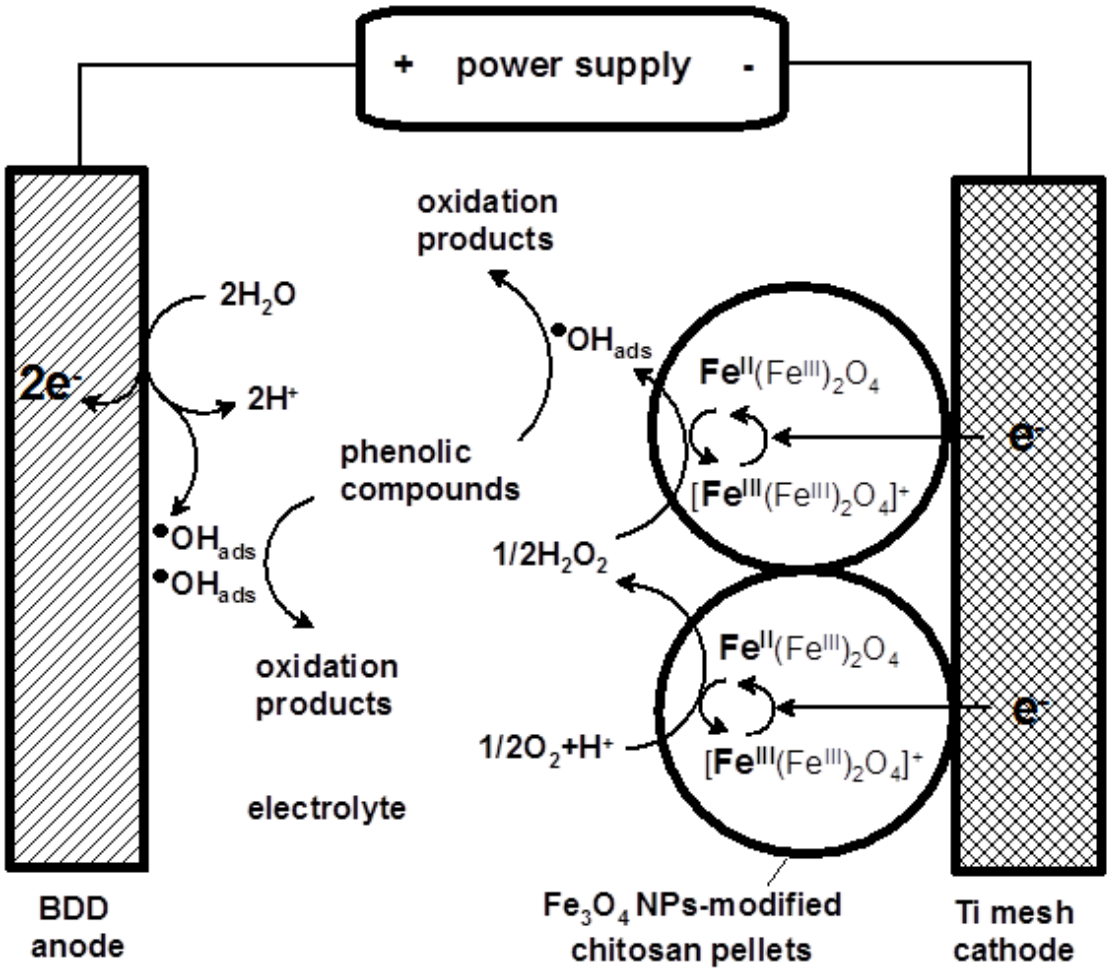
+ power supply -
oxidation products
$2H_2O$
$^{\bullet}OH_{ads}$
$Fe^{II}(Fe^{III})_2O_4$
2e-
$2H^+$
e-
phenolic compounds
$[Fe^{III}(Fe^{III})_2O_4]^+$
$^{\bullet}OH_{ads}$
$^{\bullet}OH_{ads}$
$1/2H_2O_2$
$Fe^{II}(Fe^{III})_2O_4$
oxidation products
e-
$1/2O_2+H^+$
$[Fe^{III}(Fe^{III})_2O_4]^+$
electrolyte
BDD anode
Fe_3O_4 NPs-modified chitosan pellets
Ti mesh cathode

Table 1

Pollutant	COD_i (mg dm^{-3})	COD_f (mg dm^{-3})	% η_{COD}	EC_i (mS cm^{-1})	EC_f (mS cm^{-1})
Phenol	282.50	5200.00	95	394.00	47.00
o-Chlorophenol	542.00	1250.00	57	365.00	46.40
m-Chlorophenol	249.50	4725.00	95	358.00	52.20
p-Chlorophenol	243.00	2050.00	88	370.00	46.30